Integrated Modified Repetitive Control With Disturbance Observer of Piezoelectric Nanopositioning Stages for High-Speed and Precision Motion

Zhao Feng
School of Power and Mechanical Engineering,
Wuhan University,
Wuhan 430072, China
e-mail: fengzhaozhao7@whu.edu.cn

Jie Ling
School of Power and Mechanical Engineering,
Wuhan University,
Wuhan 430072, China
e-mail: jamesling@whu.edu.cn

Min Ming
School of Power and Mechanical Engineering,
Wuhan University,
Wuhan 430072, China
e-mail: mingmin_whu@whu.edu.cn

Xiaohui Xiao[1]
School of Power and Mechanical Engineering,
Wuhan University,
Wuhan 430072, China;
Shenzhen Institute of Wuhan University,
Shenzhen 518057, China
e-mail: xhxiao@whu.edu.cn

The tracking performance of piezoelectric nanopositioning stages is vital in many applications, such as scanning probe microscopes (SPMs). Although modified repetitive control (MRC) can improve tracking performance for commonly used periodic reference input, it is sensitive to unexpected disturbances that deteriorate tracking precision, especially for high-speed motion. In order to achieve high-speed and precision motion, in this paper, a new composite control scheme by integrating MRC with disturbance observer (DOB) is developed. To simplify controller implementation, the hysteresis nonlinearity is treated as external disturbance and the proposed method is designed in frequency domain. The stability and robust stability are analyzed, and an optimization procedure to calculate the controller parameters is employed to enhance the performance to the maximum extent. To validate the effectiveness of the proposed method, comparative experiments are performed on a piezoelectric nanopositioning stage. Experimental results indicate that the hysteresis is suppressed effectively and the proposed method achieves high-speed and precision tracking with triangular waves references up to 25 Hz and improves the disturbance rejection ability with disturbances under different frequencies and robustness to model uncertainty through comparing with feedback controllers and MRC, respectively. [DOI: 10.1115/1.4042879]

1 Introduction

With the rapid development in nanotechnology, the piezoelectric nanopositioning stage becomes an essential component to achieve high-precision tracking and positioning for nanometer or subnanometer resolution in many applications, such as scanning probe microscopes (SPMs) [1], atomic force microscopes [2], micromanipulation systems [3], ultra-precision machine tools [4,5], wafer stages [6], and so on. Generally, these stages are driven by piezoelectric actuators to achieve fast response time and high stiffness, and flexure-hinge-guided mechanisms are employed to transmit motion to avoid friction [7]. The demand for high-throughput nanomanufacturing has posed new challenge for the control of high-speed and precision motion [8]. However, the indigenous hysteresis nonlinearity and lightly damped vibrational modes of piezoelectric nanopositioning stage degrade motion performance seriously.

To compensate hysteresis nonlinearity, feedforward control with inverse hysteresis model is the most common approach. The models of hysteresis are usually built by Preisach [9], Prandtl-Ishlinskii [10,11], Bouc-Wen [12] and Dahl [13] models, etc. It should be noted that in the view of practical implementation, a lot of parameters should be identified to improve the modeling accuracy. On the other hand, the cascade connection of static hysteresis nonlinearity at low-frequency region with linear vibration dynamics is a simple approach to represent the complex model of piezoelectric nanopositioning stages [14,15]. In view of this, some approaches without hysteresis modeling have been proposed by treating the hysteresis as an input disturbance [16,17]. However, with the motion speed increasing, the performance is still limited by the lightly damped modes, which restricts the operating frequency less than 1/100 to 1/10 of the first resonant mode because of oscillations and unexpected residuals [18].

In order to push the tracking performance in terms of speed, feedback controllers, such as resonant control [19], positive position feedback control [20], integral resonant control [21] and time-delay control [22], and loop-shaping approach [23] have been proposed to impart substantial damping to improve the tracking speed. Because of the fundamental algebraic restrictions in feedback, these standalone methods may not meet the required performance, such as errors caused by phase lag.

It should be noted that the periodic trajectory is commonly used in many applications, especially for the lateral motion of nanopositioning stage in SPMs [24]. To cope with the issues in this motion process, it is natural to utilize repetitive control (RC) to achieve required performance, which is based on the internal model principle [25] and can provide infinite gain at the fundamental frequency as well as its harmonics of the reference or disturbance [26]. The tracking error can converge to zero with the number of motion period increasing. RC can be plugged into an existing feedback loop to enhance performance and the periodic reference should be known primarily. Compared with another learning-type controller, iterative learning control [27], RC does not need to reset to the initial position after each iteration, which simplifies the practical implementation [28]. However, although conventional RC can handle with periodic reference or disturbance, the error at nonperiodic frequency is amplified because of waterbed effect. In Ref. [26], a dual-stage RC has been proposed to reduce the magnitude of nonperiodic frequency of the

[1]Corresponding author.

Contributed by the Dynamic Systems Division of ASME for publication in the Journal of Dynamic Systems, Measurement, and Control. Manuscript received January 14, 2018; final manuscript received January 31, 2019; published online March 25, 2019. Assoc. Editor: Srinivasa M. Salapaka.

sensitivity transfer function of the closed-loop system via cascading conventional RC with odd-harmonic RC. It should be noted that the method requires calculating parameters of both the RCs and the inverse hysteresis model. Besides, a dual-mode structure RC can handle even-harmonic periodic errors and odd-harmonic periodic errors simultaneously for constant-voltage constant frequency pulse-width modulation converters [29,30] without hysteresis nonlinearity. Recently, Chen and Tomizuka proposed a modified repetitive control (MRC) to reduce periodic errors as a repetitive disturbance observer [31]. However, the main downside of this approach lies in that it has not improved the ability to suppress nonperiodic disturbance and model uncertainties, which are common in piezoelectric nanopositioning stages stemmed by hysteresis, sensor noise, mechanical shocks, or external environment.

In the perspective of this aspect, disturbance observer (DOB) is a popular method to eliminate unexpected disturbance and model uncertainties [32]. Although a state-observer-based RC has been proposed and designed to estimate disturbance in time domain [33,34], the method is only designed for a second-order plant and the hysteresis nonlinearity for nanopositioning stages with complex dynamics is not addressed. In Ref. [35], the repeated errors are compensated through iterative learning control and additional nonrepeating exogenous signals are rejected by a H_∞ controller, where the Q filter and weighting functions are determined by the repetitive-to-nonrepetitive ratio of the collected errors calculated in frequency domain. The combined method needs to collect experimental tracking data for several iterations for one desired reference signal to compute repetitive-to-nonrepetitive off-line.

This paper is motivated to achieve high-speed and precision motion for piezoelectric nanopositioning stages with periodic reference. Although MRC can improve reference tracking performance, it is sensitive to unexpected disturbances that do not match with the frequency of reference. The main contribution of this paper is three-fold. First, in order to realize high-speed tracking and high-precision motion simultaneously, the control scheme by integrating MRC with DOB is proposed via designing it in frequency domain and treating hysteresis nonlinearity as low-frequency disturbance to simplify controller implementation. Second, the stability and robust stability of the proposed method are also analyzed and the parameters are calculated through optimization. Thirdly, the comparative experiments on a piezoelectric nanopositioning stage are performed to elucidate the ability for high-speed tracking, disturbance rejection, and robustness of the proposed method.

The rest of this paper is organized as follows. The system description is shown in Sec. 2. The controller design using MRC in tandem with DOB is presented in Sec. 3. Section 4 demonstrates the stability and parameters optimization in detail. Experiments on a piezoelectric nanopositioning stage and comparisons of the results are elaborated in Sec. 5, and Sec. 6 gives the conclusions.

2 System Description

2.1 Experimental Setup. The experimental setup is shown in Fig. 1. A piezoelectric nanopositioning stage P-561.3CD is developed to evaluate the performance. The control input voltage given through peripheral component interconnect (PCI) bus is generated by 16-bit digital to analog converters (DAC) via the data acquisition card PCI 6289 and subsequently amplified by a piezo amplifier module E-503.00 for the stage. The output position normalized and read via a sensor monitor E-509.C3A is passed to the data acquisition card PCI 6289 by 18-bit analog to digital converters (ADC). The overall control system is built in SIMULINK real-time environment on the development personal computer and executed real-time on the target personal computer. In this paper, the sample frequency of the system is set to 2 kHz.

2.2 System Identification. In order to identify the linear dynamic model of the piezoelectric nanopositioning stage without load on it, a sine-sweep input with a constant low amplitude between 0.1 Hz and 500 Hz is applied to the x axis. It should be noted that a low-amplitude voltage was used to excite the system to avoid distortion from hysteresis nonlinearity [23]. Through being discretized via zero-order holder method, the nominal linear discrete transfer function $P(z)$ with the forward time-shift operator z can be identified as

$$P(z) = \frac{0.0122z^4 - 0.045z^3 + 0.109z^2 - 0.108z + 0.0532}{z^5 - 3.794z^4 + 6.25z^3 - 5.49^2 + 2.556z - 0.5057} \quad (1)$$

The identified and measured frequency responses are plotted in Fig. 2, which indicates that Eq. (1) describes the dynamics of the stage sufficiently accurately and it contains nonminimum phase zeros. It is clear that the first resonant frequency is 210 Hz from Fig. 2, which limits the motion within a low speed when implementing the built-in feedback controller [18]. Moreover, in this paper, in order to design the proposed controller transparently, the complex dynamic of the stage is simplified by regarding the hysteresis as an external disturbance added to a linear vibration dynamic $P(z)$ to avoid hysteresis modeling [17,22,36] and the nonlinearity is migrated by the proposed method that will be verified through experiments in Sec. 5.

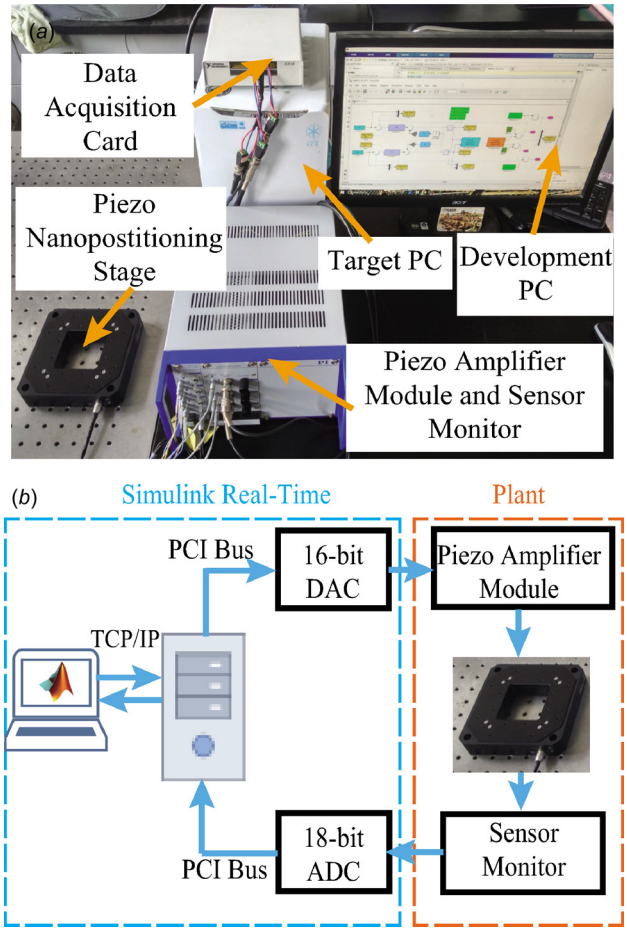

Fig. 1 The experimental setup of the piezoelectric nanopositioning stage: (*a*) experimental platform and (*b*) block diagram of control system

3 Controller Design

3.1 Modified Repetitive Control. Repetitive control is an effect control algorithm to facilitate performance with repetitive reference or disturbance based on internal model principle [25].

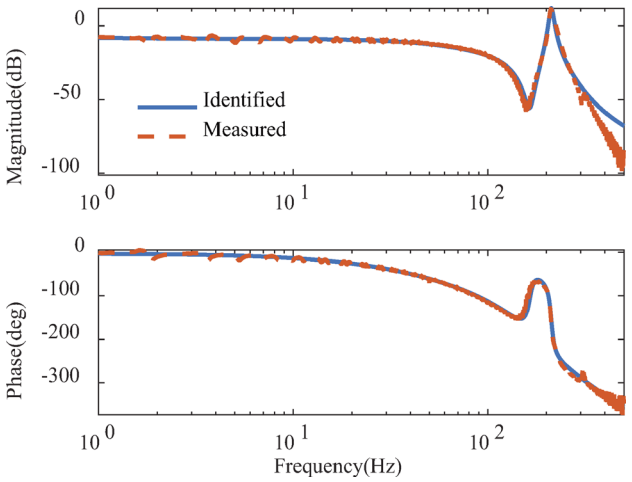

Fig. 2 Frequency response of identified and measured model with sine-sweep input

For a discrete conventional RC, a signal generator $1/(1-z^{-N})$, where N is the number of points per period of the reference or disturbance, should be contained in the feedback loop. However, the method magnifies the undesired gain at other frequencies according to Bode integral theorem [37]. For precision motion, the nonperiodic disturbance can be obvious, so that the tracking performance is deteriorated significantly.

In this paper, a MRC proposed by Chen and Tomizuka [31] is utilized to alleviate the gain amplifications at the nonperiodic frequencies. The block diagram is demonstrated in Fig. 3, where $C_{\text{fb}}(z)$ is the baseline feedback controller, $P^{-1}(z)$ is the model inversion of the nominal plant $P(z)$ and $Q_{\text{RC}}(z)$ is a spectrum extractor filter to provide infinite gains at the harmonics of the periodic reference. The signal $r(k)$ is the anticipated periodic reference, $y(k)$ is the position output, and $e(k)$ is the tracking error with sensor noise $n(k)$. The control force $u(k)$ is determined by both feedback controller and MRC. It should be noted that $d(k)$ contains hysteresis nonlinearity, external unknown disturbance, and error caused by model uncertainties, which should be taken into consideration for piezoelectric nanopositioning systems.

For a nonminimum phase system $P(z)$, the transfer function can be decomposed as

$$P(z) = \frac{B_s(z)B_u(z)}{A(z)} \tag{2}$$

where $B_s(z)$, $B_u(z)$ are composed by stable and unstable zeros, respectively, and $A(z)$ contains all the identified poles. $B_u(z)$ is a nth-order polynomial with n nonminimum phase zeros and expressed as

$$B_u(z) = b_{un}z^n + b_{u(n-1)}z^{n-1} + \cdots b_{u0} \tag{3}$$

The zero-phase-error tracking controller [38,39] is adopted to approximate the inversion of $P(z)$ in this paper, i.e.,

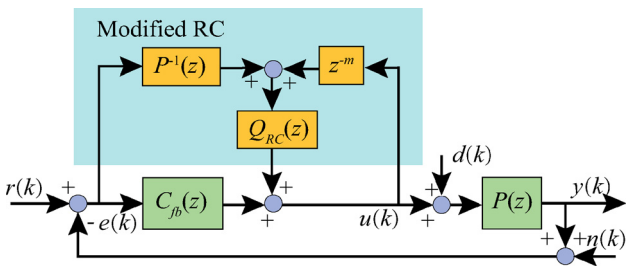

Fig. 3 Block diagram of MRC with a series–parallel implementation

$$P^{-1}(z) = \frac{A(z)B_u^f(z)z^{-(n+d)}}{B_s(z)\left(B_u(z)|_{z=1}\right)^2} \tag{4}$$

where d is the delay to make the transfer function casual for practical implementation. $B_u^f(z)$ is a nth-order polynomial by flipping the coefficients of $B_u(z)$, i.e.,

$$B_u(z) = b_{u0}z^n + b_{u1}z^{n-1} + \cdots b_{un} \tag{5}$$

Therefore, for $m = d + n$, it can be obtained that

$$P(z)P^{-1}(z) \approx z^{-m} \tag{6}$$

According to Fig. 3, the equivalent controller from $e(k)$ to $u(k)$ is

$$C(z) = \frac{C_{\text{fb}}(z) + Q_{RC}(z)P^{-1}(z)}{1 - z^{-m}Q_{RC}(z)} \tag{7}$$

and the sensitivity transfer function $S_{\text{RC}}(z)$ from $r(k)$ to $e(k)$ is given by

$$S_{\text{RC}}(z) = \frac{1 - z^{-m}Q_{\text{RC}}(z)}{1 + P(z)C_{\text{fb}}(z) + Q_{\text{RC}}(z)\left(P^{-1}(z)P(z) - z^{-m}\right)} \tag{8}$$

From Eq. (6), $S_{\text{RC}}(z)$ satisfies that

$$S_{\text{RC}}(z) \approx \frac{1 - z^{-m}Q_{\text{RC}}(z)}{1 + P(z)C_{\text{fb}}(z)} \tag{9}$$

In order to obtain infinite gains at the harmonics of $r(k)$, $Q_{RC}(z)$ is designed as [31]

$$Q_{\text{RC}}(z) = \frac{(1-\alpha)z^{-(N-m)}}{1 - \alpha z^{-N}} \tag{10}$$

where $\alpha \subset [0, 1)$ is the parameter make MRC more flexible. The numerator of Eq. (9) is expressed as

$$1 - z^{-m}Q_{\text{RC}}(z) = \frac{1 - z^{-N}}{1 - \alpha z^{-N}} \tag{11}$$

According to Eq. (11), if $\alpha = 0$, the MRC generates a loop shape that is similar to a traditional RC, which may amplify nonperiodic errors. On the other hand, $\alpha = 1$ cuts off the control force of the repetitive compensation. When $\alpha \subset [0, 1)$, the frequency response of Eq. (11) demonstrates that as α increasing, the signal passed through is selected at the harmonics of the periodic reference and both the repetitive and unexpected errors are significantly alleviated. However, a smaller α results in a faster convergence with amplification of nonperiodic errors and vise verse [31,36].

To improve the robustness of MRC caused by model uncertainties at high-frequency region, a zero phase low-pass filter is added to $Q_{\text{RC}}(z)$ as

$$Q_{\text{robust}}(z) = az^{-1} + b + az \tag{12}$$

and a and b should satisfy $2a + b = 1$. Therefore, the $Q_{\text{RC}}(z)$ utilized in this paper is described as

$$Q_{\text{RC}}(z) = \frac{(1-\alpha)(az^{-1} + b + az)z^{-(N-m)}}{1 - \alpha z^{-N}} \tag{13}$$

Remark 1. Although MRC can handle with repetitive errors without amplification of nonperiodic disturbance, the ability to reject disturbance is still limited, which can be deduced from the transfer function from $d(k)$ to $y(k)$, i.e.,

$$G_{\text{RC},yd}(z) \approx \frac{P(z)(1 - z^{-m}Q_{\text{RC}}(z))}{1 + P(z)C_{\text{fb}}(z)} \tag{14}$$

For the best situation with $\alpha = 0.99$, the disturbance rejection of MRC is at the same level as feedback controller. Note that in piezoelectric nanopositioning stage with high-precision motion, the implementation with standalone MRC may not be sufficient to handle hysteresis nonlinearity, low-frequency errors, and external unknown nonperiodic disturbance, especially for high-speed tracking.

3.2 Disturbance Observer. In the context of external disturbance and system uncertainties, DOB is an effective method by augmenting into the original feedback controller as the inner loop to estimate the disturbance and feeds it back to original control force to achieve disturbance rejection [25,40,41]. The block diagram of DOB with outer feedback loop is illustrated in Fig. 4, where $u_{\text{fb}}(k)$ is control signal of feedback controller, $d_{\text{est}}(k)$ is the estimated disturbance of $d(k)$ and $Q_{\text{DOB}}(z)$ is a low-pass filter to retain robustness. According to Fig. 4, the transfer function from $u_{\text{fb}}(k)$ to $y(k)$ without the feedback loop is deduced as

$$G_{\text{DOB},yu_{\text{fb}}}(z) = \frac{P(z)}{1 + Q_{\text{DOB}}(z)\left(P(z)P^{-1}(z) - z^{-m}\right)} \tag{15}$$

and the disturbance rejection ability with feedback controller $C_{\text{fb}}(z)$ is concluded by

$$G_{\text{DOB},yd}(z) = \frac{P(z)(1 - z^{-m}Q_{\text{DOB}}(z))}{1 + P(z)C_{fb}(z) + Q_{\text{DOB}}(z)\left(P(z)P^{-1}(z) - z^{-m}\right)} \tag{16}$$

It is obvious that with a low-pass filter $Q_{\text{DOB}}(z)$, the system performs approximately as the nominal plant $P(z)$ and the disturbance within the filter bandwidth can be compensated according to Eq. (16). Although the observed disturbance exits m-step delay, the amplitude response of $1 - z^{-m}Q_{\text{DOB}}$ is zero if $Q_{\text{DOB}} = 1$ under the ideal condition. However, it should be noted that DOB can compensate the disturbance within the bandwidth of $Q_{\text{DOB}}(z)$ considering that a compromise should be made for the robustness of the plant and noise.

Remark 2. With Eq. (6), the transfer function from $r(k)$ to $e(k)$with feedback controller is simply expressed as

$$G_{\text{DOB},er}(z) \approx \frac{1}{1 + P(z)C_{\text{fb}}(z)} = S_{\text{fb}}(z) \tag{17}$$

which infers that the tracking performance has not been improved significantly and its frequency domain behavior is similar to sensitivity transfer function with feedback controller $S_{\text{fb}}(z)$ although DOB can improve the ability for disturbance rejection of the system.

3.3 Integration of Modified Repetitive Control With Disturbance Observer. For piezoelectric nanopositioning stage with periodic reference, it is necessary to achieve high-speed and precision motion simultaneously in order to satisfy the requirement for practical application. In this paper, a composite control

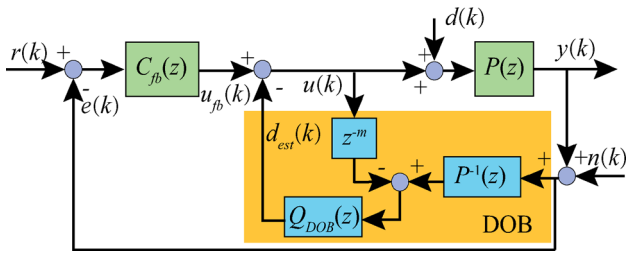

Fig. 4 Block diagram of DOB with a series–parallel implementation

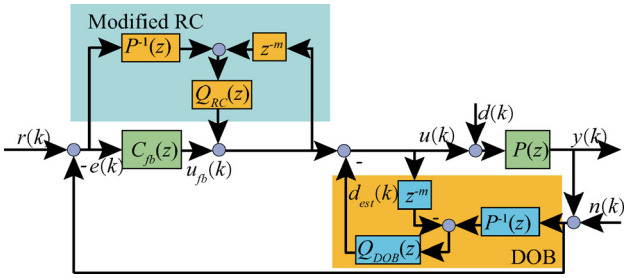

Fig. 5 Block diagram of the proposed control scheme by integrating MRC with DOB

scheme by integrating MRC with DOB is proposed to handle this issue as is shown in Fig. 5.

Based on the block diagram, the following input–output relationships can be derived and the forward time-shift operator z is omitted for brevity

$$G_{er} = \frac{\left(1 + Q_{\text{DOB}}(PP^{-1} - z^{-m})\right)(1 - z^{-m}Q_{\text{RC}})}{1 + PC_{\text{fb}} + (Q_{\text{RC}} + Q_{\text{DOB}} - z^{-m}Q_{\text{RC}}Q_{\text{DOB}})(PP^{-1} - z^{-m})} \tag{18}$$

$$G_{yd} = \frac{P(1 - z^{-m}Q_{\text{DOB}})(1 - z^{-m}Q_{\text{RC}})}{1 + PC_{\text{fb}} + (Q_{\text{RC}} + Q_{\text{DOB}} - z^{-m}Q_{\text{RC}}Q_{\text{DOB}})(PP^{-1} - z^{-m})} \tag{19}$$

Taking Eq. (6) into consideration, the amplitude responses of transfer functions with different choices of the Q filter are demonstrated in Table 1 to further elucidate the superiority of the proposed method. It is clear that when $Q_{\text{RC}} = 1$, $Q_{\text{DOB}} = 0$, the reference is perfectly tracked but the disturbance has not been rejected unless the frequency of disturbance locates at the harmonics of the periodic reference. On the other hand, the disturbance can be completely compensated with $Q_{\text{RC}} = 0$, $Q_{\text{DOB}} = 1$. However, the tracking performance is not improved significantly. As a consequence, considering the multiple objectives, including high-speed tracking, precision motion, and disturbance rejection, the proposed method can achieve the required performance substantially via choosing $Q_{\text{RC}} = 1$, $Q_{\text{DOB}} = 1$. In order to improve the performance as much as possible, the design of Q_{RC} and Q_{DOB} is of great importance. According to Eqs. (18) and (19), it is nature that the bandwidth of Q_{robust} both in MRC and Q_{DOB} should be as large as possible to achieve high-speed tracking and reject disturbance within larger frequency region on the premise that the overall system retain stability.

Remark 3. Compared with the integrated method designed in time domain proposed in Refs. [33] and [34], the proposed method in this paper is developed in frequency domain, which can be easily implemented digitally via high-speed data acquisition. Besides, the above-mentioned method is only designed for a second-order plant and the hysteresis nonlinearity is not addressed, which is unavoidable for piezoelectric nanopositioning stages. On the other hand, the improvement of rejecting nonperiodic and

Table 1 Comparisons of amplitude responses with different *Q* filters

Q filter	$\lvert G_{er}\rvert$	$\lvert G_{yd}\rvert$
$Q_{\text{RC}} = 0, Q_{\text{DOB}} = 0$	$\left\lvert \frac{1}{1 + PC_{\text{fb}}} \right\rvert$	$\left\lvert \frac{P}{1 + PC_{\text{fb}}} \right\rvert$
$Q_{\text{RC}} = 1, Q_{\text{DOB}} = 0$	0	$\left\lvert \frac{P(1 - z^{-m}Q_{\text{RC}})}{1 + PC_{\text{fb}}} \right\rvert$
$Q_{\text{RC}} = 0, Q_{\text{DOB}} = 1$	$\left\lvert \frac{1}{1 + PC_{\text{fb}}} \right\rvert$	0
$Q_{\text{RC}} = 1, Q_{\text{DOB}} = 1$	0	0

low-frequency disturbance is enhanced substantially for high-speed and precision tracking in this paper, which is different from the controller in Ref. [36].

Remark 4. In essence, the control scheme is a double DOB controller constituted by a repetitive DOB, i.e., MRC and a frequency DOB to minimize error and reject disturbance, respectively. Note that the baseline controller $C_{\text{fb}}(z)$ can either remain unchanged or be replaced by other various control approaches for the plug-in property of the proposed method.

4 Stability and Parameters Optimization

4.1 Stability and Robust Stability. For practical implementation, it is necessary to analyze the stability of the proposed method, which is demonstrated as follows.

THEOREM 1 (Stability). *Assume that the baseline feedback controller $C_{fb}(z)$ can stabilize the closed-loop system, i.e., the sensitivity transfer function $S_{fb}(z)$ is stable and T_s is the sample time. If the Q filters meet*

$$|Q_{\text{RC}} + Q_{\text{DOB}} - z^{-m}Q_{\text{RC}}Q_{\text{DOB}}|_{z=e^{j\omega T_s}} < \left|\frac{1+PC_{fb}}{PP^{-1}-z^{-m}}\right|_{z=e^{j\omega T_s}} \tag{20}$$

for $\omega \subset [0, \pi/T_s]$, the system with the proposed method is asymptotically stable.

Proof. The transfer function from $r(k)$ to $y(k)$ is derived according to Fig. 5 as

$$G_{yr} = \frac{PC_{fb} + PP_n^{-1}Q_{\text{RC}}}{1 + PC_{\text{fb}} + (Q_{\text{RC}} + Q_{\text{DOB}} - z^{-m}Q_{\text{RC}}Q_{\text{DOB}})(PP^{-1} - z^{-m})} \tag{21}$$

After rearrangement, Eq. (21) can be restated as the product of three simpler transfer functions as

$$G_{yr} = H_2 \frac{1}{1 + S_{\text{fb}}H_1} \tag{22}$$

with

$$H_1 = (Q_{\text{RC}} + Q_{\text{DOB}} - z^{-m}Q_{\text{RC}}Q_{\text{DOB}})(PP^{-1} - z^{-m}) \tag{23}$$

$$H_2 = \frac{PC_{\text{fb}} + PP^{-1}Q_{\text{RC}}}{S_{\text{fb}}} \tag{24}$$

The equivalent block diagram of Eq. (22) is shown in Fig. 6. According to small gain theorem [42], the condition for stability should satisfy

$$|S_{\text{fb}}H_1|_{z=e^{j\omega T_s}} < 1 \tag{25}$$

for $\omega \subset [0, \pi/T_s]$. Because S_{fb} is always stable, Eq. (25) can be reformulated as

$$|Q_{\text{RC}} + Q_{\text{DOB}} - z^{-m}Q_{\text{RC}}Q_{\text{DOB}}|_{z=e^{j\omega T_s}} < \left|\frac{1}{S_{\text{fb}}(PP^{-1} - z^{-m})}\right|_{z=e^{j\omega T_s}} \tag{26}$$

Therefore, Eq. (22) meets the stability condition of the closed-loop system with the proposed method.

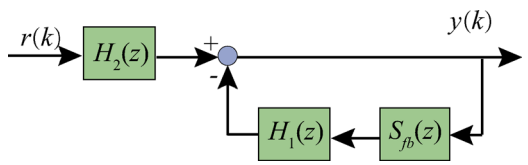

Fig. 6 Equivalent block diagram for stability analysis

In terms of the robustness, another challenge of the stage is that the first resonant mode frequency varied with the load on it, which may result in the unstable closed-loop system. The robust stability considered the model uncertainty of the proposed controller as follows.

THEOREM 2 (Robust stability). *Assume that the baseline feedback controller $C_{fb}(z)$ can stabilize the closed-loop system and the perturbed plant is determined by $P_u = P(1 + \Delta W)$, where ΔW is the determined bound of the multiplicative model uncertainty. The sufficient robust stability of the closed-loop system is given by*

$$|\Delta W|_{z=e^{j\omega T_s}} < \left|\frac{D_{yr}}{PC_{fb} + PP^{-1}Q}\right|_{z=e^{j\omega T_s}} \tag{27}$$

for $\omega \subset [0, \pi/T_s], Q = Q_{RC} + Q_{DOB} - z^{-m}Q_{RC}Q_{DOB}$, and D_{yr} is the denominator of G_{yr}

Proof. Substituting $P_u = P(1 + \Delta W)$ into the denominator of G_{yr}, the characteristic equation of the system with P_u can be deduced as

$$D_{yr,u} = 1 + P(1 + \Delta W)C_{\text{fb}} + (P(1 + \Delta W)P^{-1} - z^{-m})Q \tag{28}$$

Rearrange the term and Eq. (28) can be rewritten as

$$D_{yr,u} = D_{yr} + \left(1 + \frac{PC_{\text{fb}} + PP^{-1}Q}{D_{yr}}\Delta W\right) \tag{29}$$

Based on small gain theorem [42], the condition for the robust stability of the system is expressed as

$$\left|\frac{PC_{\text{fb}} + PP^{-1}Q}{D_{yr}}\Delta W\right|_{z=e^{j\omega T_s}} < 1 \tag{30}$$

4.2 Parameters Optimization. The analysis in Sec. 3, it is clear the bandwidths of Q_{RC} and Q_{DOB} affect the performance significantly. However, because the Q filters in the proposed method contains low-pass filters, the cutoff frequencies are limited by the robust stability and precision tracking performance at high frequencies. In this paper, in order to exert the control force of the controller as much as possible, a simple optimization procedure is employed to determine the bandwidth of the low-pass filters with the constrain of stability. The optimization problem is expressed as

$$\max_{\omega_{\text{RC}},\omega_{\text{DOB}}} \ \omega_{\text{RC}} + \omega_{\text{DOB}}$$

$$s.t.$$

$$\begin{cases} Q_{\text{robust}}(z)|_{z=e^{j\omega_{\text{RC}}T_s}} = 0.701 \\ Q_{\text{DOB}}(z)|_{z=e^{j\omega_{\text{DOB}}T_s}} = 0.701 \\ |Q|_{z=e^{j\omega T_s}} < \left|\dfrac{1+PC_{\text{fb}}}{PP^{-1}-z^{-m}}\right|_{z=e^{j\omega T_s}} \\ |\Delta W|_{z=e^{j\omega T_s}} < \left|\dfrac{D_{yr}}{PC_{fb}+PP^{-1}Q}\right|_{z=e^{j\omega T_s}} \\ 0 < \omega_{\text{RC}}, \omega_{\text{DOB}} < 2\pi f_{\text{Nyquist}} \end{cases} \tag{31}$$

where ω_{RC}, ω_{DOB} are the cutoff frequencies of low-pass filter in MRC and DOB, respectively. f_{Nyquist} is the Nyquist frequency calculated by $2/T_s$. According to Eq. (31), the cutoff frequencies are optimized simultaneously under the condition for retaining stability and robust stability to enhance the performance to the maximum extent.

5 Experimental Results and Analysis

In this section, controller implementation and comparative experiments are demonstrated to verify the performance of the

proposed method. Furthermore, four controllers have been developed for comparisons as follows:

(1) $\boldsymbol{C}_1$: the baseline feedback controller with a lower bandwidth.
(2) $\boldsymbol{C}_2$: the baseline feedback controller with a higher bandwidth.
(3) $\boldsymbol{C}_3$: the baseline feedback controller $\boldsymbol{C}_1$ with MRC.
(4) $\boldsymbol{C}_4$: the baseline feedback controller $\boldsymbol{C}_1$ with the proposed composite method.

5.1 Controller Implementation. For the baseline feedback controller, a notch filter with integral controller is designed primarily. Through being discretized by zero-order holder method, it is expressed as

$$C_{\text{fbl}} = \frac{0.06251z^3 - 0.03651z^2 - 0.03834z + 0.06068}{z^3 - 2.111z^2 + 1.963z - 0.8519} \tag{32}$$

In addition, another feedback controller with a higher closed-loop bandwidth is designed to validate the effectiveness of the proposed controller through comparison, i.e.,

$$C_{\text{fbh}} = \frac{0.1042z^3 - 0.06085z^2 - 0.06391z + 0.1011}{z^3 - 2.111z^2 + 1.963z - 0.8519} \tag{33}$$

For the implementation of the proposed method, the bound of multiplicative model uncertainty ΔW of the stage is identified first. Figure 7 demonstrates the frequency responses of the multiplicative model uncertainty with different loads as the load on the stage increasing from 0 g to 300 g with sine-sweep input and the ΔW is expressed as

$$\Delta W = \frac{2.512z^4 - 8.568z^3 + 10.96z^2 - 6.235z + 1.331}{z^4 - 2.693z^3 + 2.72z^2 - 1.221z + 0.2056} \tag{34}$$

The control scheme in Fig. 5 is adopted for the optimization process. The plant inversion $P^{-1}(z)$ is calculated by zero-phase-error tracking controller using Eq. (4), and the delay term m is determined via $m = d + n$. Combined with Eq. (31) and the transfer function ΔW, the optimization process can be conducted in MATLAB by the function *fmincon* for given constraints. According to the optimization result, the cutoff frequencies of the low-pass filters are obtained as 363 Hz with $a = 0.25$, $b = 0.5$ in Q_{RC} and 153 Hz for a third-order Butterworth filter in Q_{DOB}, respectively. It should be noted that a time-varying α is designed for fast convergence and small steady-state error [31]. In this paper, for the first period of the reference, α is set as 0.001 to achieve fast convergence, then increased to 0.9 for the next two periods, and finally kept at 0.9.

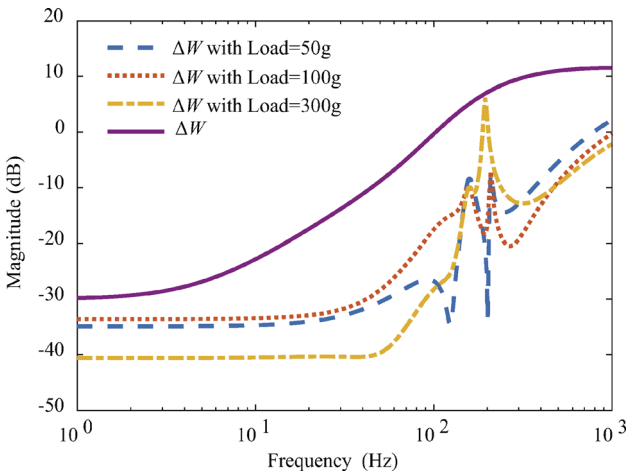

Fig. 7 Multiplicative model uncertainty with different loads and the bound of uncertainty ΔW

To investigate the superiority of the proposed method in frequency domain, the Bode diagrams of transfer functions from $r(k)$ to $y(k)$, $r(k)$ to $e(k)$ and $d(k)$ to $y(k)$ are plotted in Fig. 8 with $\alpha = 0.99$, $N = 100$ and 2 kHz sample rate. It is clear that the bandwidth of $\boldsymbol{C}_2$ at 40.8 Hz is higher that of at 17.2 Hz $\boldsymbol{C}_1$ at the expense of light overshoot. From Fig. 8(*b*), the magnitudes of $\boldsymbol{C}_3$ and $\boldsymbol{C}_4$ have lower gains at the harmonics of 20 Hz compared with $\boldsymbol{C}_1$ and $\boldsymbol{C}_2$, i.e., the frequency of reference, which indicates that the reference caused tracking error is eliminated to achieve precision tracking. However, it should be noted that the disturbance rejection ability of $\boldsymbol{C}_3$ is the same as $\boldsymbol{C}_1$ aside from the disturbance locating at the harmonics of the reference as is illustrated in Fig. 8(*c*). In practice, the standalone implementation of $\boldsymbol{C}_3$ may be not sufficient under large external disturbance such as model uncertainty and unknown nonperiodic disturbance from environment. By contrast, it can be concluded that $\boldsymbol{C}_4$ can reject disturbance significantly and maintain precision tracking simultaneously from frequency domain analysis.

5.2 Comparative Experiments

5.2.1 Suppression of Hysteresis. In this paper, the hysteresis nonlinearity is treated as a low-frequency external disturbance without building hysteresis modeling for simple implementation. Experimental results of hysteresis curves with different controllers are displayed in Fig. 9 when 1 Hz triangular wave with 5 μm peak-to-peak amplitude is injected into x axis. For the open-loop

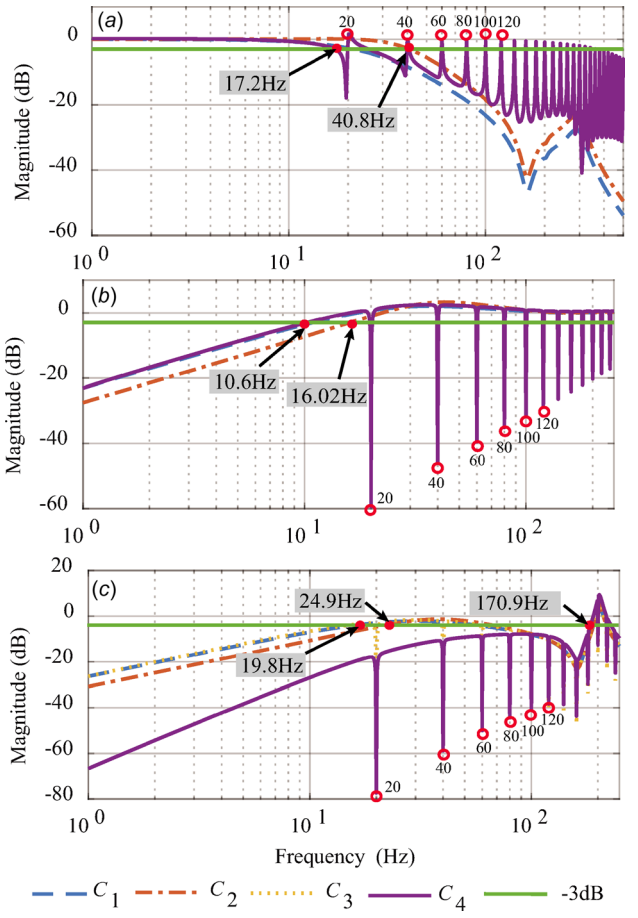

Fig. 8 Comparisons in frequency domain of different controllers: (*a*) Bode diagram of transfer functions from $r(k)$ to $y(k)$, (*b*) Bode diagram of transfer functions from $r(k)$ to $e(k)$, and (*c*) Bode diagram of transfer functions from $d(k)$ to $y(k)$

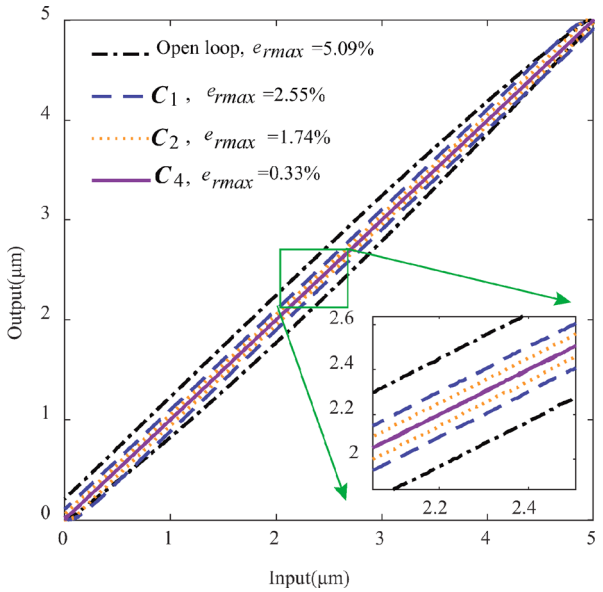

Fig. 9 Experimental results of hysteresis suppression with different controllers

Table 2 Statistical results of steady-state errors with different references

Error (nm)		C_1	C_2	C_3	C_4
5 Hz	e_{rms}	509.230	271.328	3.814	3.198
	e_{max}	596.730	394.881	20.200	16.075
10 Hz	e_{rms}	964.990	550.508	6.841	4.454
	e_{max}	1146.100	773.208	39.401	31.302
20 Hz	e_{rms}	1613.801	1122.414	11.974	11.662
	e_{max}	2194.002	1509.803	68.315	63.216
25 Hz	e_{rms}	1775.101	1449.699	15.942	15.547
	e_{max}	2601.102	1904.375	79.282	79.281

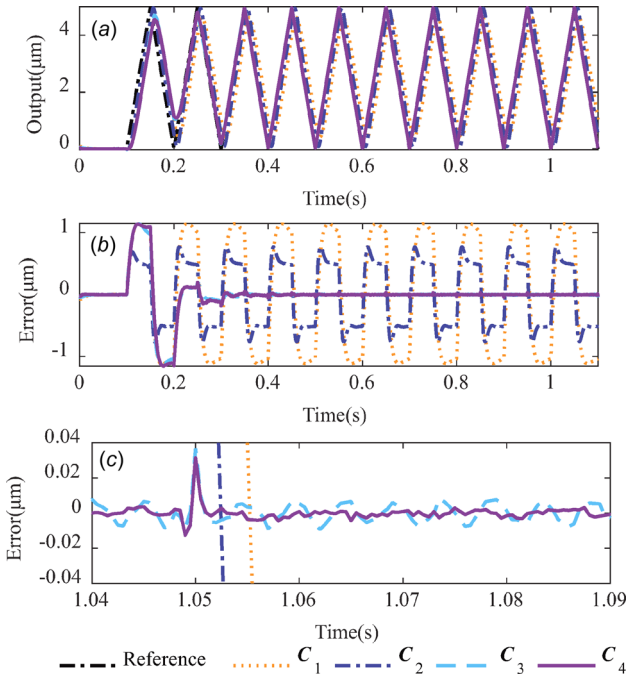

Fig. 10 Experimental results of 10 Hz triangular wave tracking with different controllers: (*a*) tracking results, (*b*) tracking errors, and (*c*) zoomed-in view of the steady-state tracking error

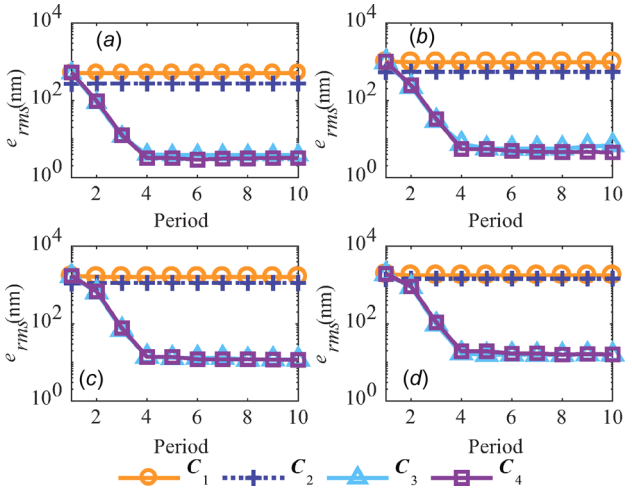

Fig. 11 Experimental results of e_{rms} versus period with different controllers: (*a*) 5 Hz triangular wave, (*b*) 10 Hz triangular wave, (*c*) 20 Hz triangular wave, and (*d*) 25 Hz triangular wave

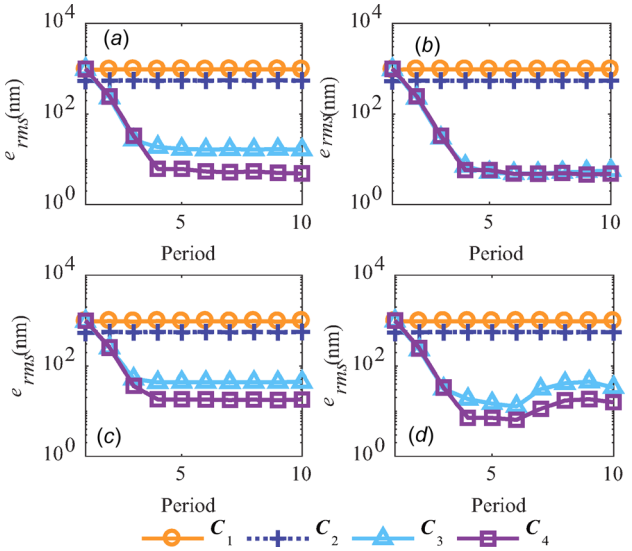

Fig. 12 Experimental results of e_{rms} versus period with different disturbances: (*a*) tracking error under $d_1(k)$, (*b*) tracking error under $d_2(k)$, (*c*) tracking error under $d_3(k)$, and (*d*) tracking error under $d_4(k)$

tracking, the relative maximal error (e_{rmax}) is 5.09%, which exhibits its obvious hysteresis nonlinearity. Note that although the stand-alone feedback controllers C_1 and C_2 can suppress hysteresis partly, the e_{rmax} of 2.55% and 1.74% are still large for precision tracking. The effectiveness of the proposed method C_4 is verified by the e_{rmax} of 0.33%, which demonstrates that the hysteresis is mitigated substantially.

5.2.2 High-Speed Trajectory Tracking. In order to validate the high-speed tracking performance of the proposed method, the triangular waves at 5 Hz, 10 Hz, 20 Hz, and 25 Hz over a 5 μm displacement range are performed on the piezoelectric nanopositioning stage. The steady-state root-mean-square errors (e_{rms}) and maximal errors (e_{max}) are tabulated in Table 2 in detail. As an illustration, the tracking performance with 10 Hz triangular waves is demonstrated in Fig. 10 in detail. The e_{rms} and e_{max} with C_4 reduce 34.89% (from 6.841 nm to 4.454 nm) and 20.56% (from 39.401 nm to 31.302 nm), respectively, with respect to the condition with C_3, whereas C_1 and C_2 cannot achieve the anticipated results.

Table 3 Statistical results of steady-state errors with different disturbances

Error (nm)		C_1	C_2	C_3	C_4
$d_1(k)$	e_{rms}	957.850	546.438	16.319	4.871
	e_{max}	1137.140	767.668	56.688	31.026
$d_2(k)$	e_{rms}	963.760	548.172	5.665	4.843
	e_{max}	1152.891	762.052	38.240	30.330
$d_3(k)$	e_{rms}	970.870	554.743	44.435	18.060
	e_{max}	1146.670	775.261	88.670	53.200
$d_4(k)$	e_{rms}	962.760	551.009	33.494	15.780
	e_{max}	1142.310	784.888	90.075	45.181

The e_{rms} of each period are showed in Fig. 11. It is can be seen that the performance with $\boldsymbol{C}_1$ is the worst especially at the frequencies of references above 5 Hz, i.e., the standalone feedback controller cannot handle with high-speed tracking. $\boldsymbol{C}_2$ is better than $\boldsymbol{C}_1$ for its higher sensitivity function bandwidth of 10.6 Hz and 16.02 Hz, respectively. For $\boldsymbol{C}_3$ and $\boldsymbol{C}_4$, the e_{rms} and e_{max} decrease within 16 nm and 80 nm, respectively, during all the tracking references, which shows that the performance improves significantly. According to Fig. 11 and Table 2, the results of $\boldsymbol{C}_3$ and $\boldsymbol{C}_4$ are very similar and the key difference between them lies in that a DOB is included in $\boldsymbol{C}_4$. It should be noted that the experiments are conducted in ideal laboratory environment, where the external disturbance is isolated perfectly. Despite this, the performance still improves lightly with the proposed method. As can be observed, the proposed method can remain precision even at high-speed tracking.

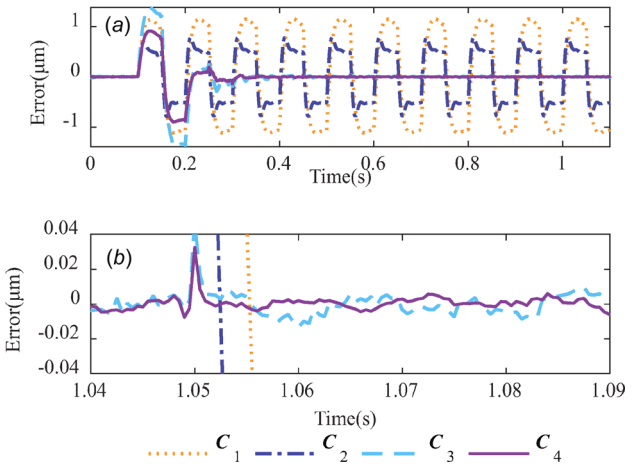

Fig. 14 Experimental results of 10 Hz triangular wave tracking with 300 g load: (*a*) tracking errors and (*b*) zoomed-in view of the steady-state tracking error

5.2.3 Disturbance Rejection. To investigate the disturbance rejection of the proposed method, four different disturbances are injected to the system to simulate the possible conditions in real implementation, which are define as

$$\begin{cases} d_1(k) = 0.05\sin(2\pi 5k) \\ d_2(k) = 0.05\sin(2\pi 10k) \\ d_3(k) = 0.05\sin(2\pi 15k) \\ d_4(k) = \text{Chirp Disturbance} \end{cases} \tag{35}$$

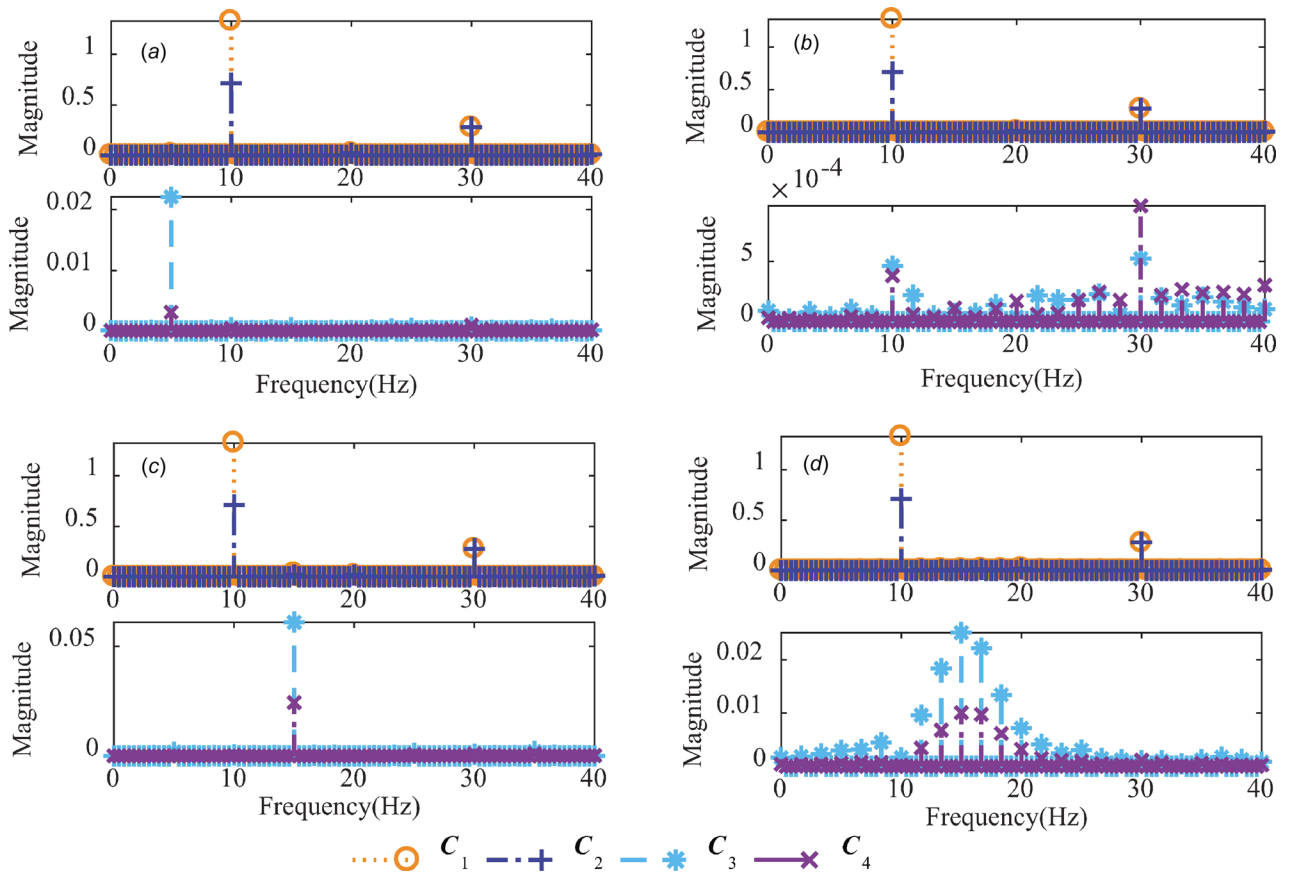

Fig. 13 Spectrum of steady-state errors with different disturbances: (*a*) steady-state error under $d_1(k)$, (*b*) steady-state error under $d_2(k)$, (*c*) steady-state error under $d_3(k)$, and (*d*) steady-state error under $d_4(k)$

Table 4 Statistical results of steady-state errors with 300 g load

Error (nm)		C_1	C_2	C_3	C_4
300 g	e_{rms}	965.404	551.148	7.405	4.538
	e_{max}	1155.122	783.263	47.796	32.506

For simplification, $d_1(k)$, $d_2(k)$, and $d_3(k)$ are periodic signals, and $d_4(k)$ a chirp disturbance with frequency varying from 0.01 Hz to 20 Hz that is defined as a time-varying signal. The unit of the above-mentioned disturbances is μm.

Figure 12 shows the performance of each period with different disturbances when the reference is a 10 Hz triangular wave and the statistical errors are given in Table 3. The conditions with $\boldsymbol{C}_1$ and $\boldsymbol{C}_2$ exhibit the worse performance, which is the same as trajectory tracking. Theoretically, the performance of $\boldsymbol{C}_3$ for $d_1(k)$, $d_3(k)$, and $d_4(k)$ should be close to $\boldsymbol{C}_1$ according to Table 2. Because $\boldsymbol{C}_3$ can compensate the error caused by delay with $\boldsymbol{C}_1$ at high-speed tracking, its performance is superior to standalone feedback controller $\boldsymbol{C}_1$. For $d_2(k)$, the frequency of this disturbance locates at the fundamental frequency of the periodic reference, which presents the best performance for both $\boldsymbol{C}_3$ and $\boldsymbol{C}_4$. Compared with $\boldsymbol{C}_3$, $\boldsymbol{C}_4$ can cope with different disturbances no matter the frequency of disturbance matches with the reference or not. Even for the time-varying disturbance $d_4(k)$, the e_{rms} and e_{max} with $\boldsymbol{C}_4$ reduce 52.89% (from 33.494 nm to 15.780 nm) and 49.51% (from 90.075 nm to 45.181 nm), respectively, with respect to the condition with $\boldsymbol{C}_3$. The spectra of steady-state errors with different disturbances are demonstrated in Fig. 13. It is clear that for $\boldsymbol{C}_1$ and $\boldsymbol{C}_2$ the frequency components of errors mainly locate at the harmonics of the reference, whereas $\boldsymbol{C}_3$ and $\boldsymbol{C}_4$ can compensate errors at those frequencies effectively. Furthermore, errors caused by nonperiodic disturbance can also be suppressed significantly with the proposed method, which is evident in Figs. 13(*a*), 13(*c*), and 13(*d*) compared with $\boldsymbol{C}_3$.

5.2.4 Robustness Test. The performance of the proposed controller to model uncertainty is also conducted. In this subsection, the 10 Hz triangular signals are fed into the closed-loop system with different controllers to test the robust stability for the stage with 300 g load. Note that the proposed controller in this paper is designed for the unloaded model and its parameters remain unchanged during the experiments. The tracking performances with different loads are plotted in Fig. 14 and the statistical results of errors are recorded in Table 4. It is evident that the proposed controller achieves the best performance and the e_{rms} of feedback only controllers $\boldsymbol{C}_1$ and $\boldsymbol{C}_2$ still exceed 500 nm. For $\boldsymbol{C}_3$, the e_{rms} and e_{max} are 7.405 nm and 47.796 nm, respectively. In comparison with that, the statistical errors improve 38.72% (from 7.405 nm to 4.538 nm) and 31.99% (from 47.796 nm to 32.506 nm), which demonstrates that the proposed method can handle with model uncertainty and achieve a better tracking performance.

6 Conclusions

In this paper, a composite control scheme by integrating MRC with DOB is proposed to achieve high-speed and precision motion simultaneously for piezoelectric nanopositioning stages with periodic reference even under unexpected disturbance. The hysteresis nonlinearity is treated as low-frequency disturbance to avoid hysteresis modeling and simplify controller implementation and the proposed method is developed in frequency domain. Furthermore, the stability and robust stability are analyzed rigorously and the parameters are calculated through optimization to enhance the performance mostly. Although MRC can compensate the disturbance with frequency at the harmonics of reference, the disturbance rejection ability is not improved at other frequency region. To validate the performance, the proposed method is also performed on a piezoelectric nanopositioning stage. Experimental results show that the proposed method can suppress low-frequency hysteresis effectively and achieve the best performance with the triangular waves references up to 25 Hz, disturbances of different frequencies, and model uncertainty caused by loads on the stage through comparing with various controllers.

The future work will concentrate on designing the inverse model using nonmodel-based approach and extent this approach to multiple-input–multiple-output systems.

Funding Data

- China Postdoctoral Science Foundation (Grant No. 2018M642905; Funder ID: 10.13039/501100002858).
- Shenzhen Science and Technology Program (Grant No. JCYJ20170306171514468; Funder ID: 10.13039/501100010877).

References

[1] Salapaka, S. M., and Salapaka, M. V., 2015, "Scanning Probe Microscopy," Control Syst. IEEE, **28**(2), pp. 65–83.
[2] Yong, Y. K., and Fleming, A. J., 2016, "High-Speed Vertical Positioning Stage With Integrated Dual-Sensor Arrangement," Sens. Actuators A Phys., **248**, pp. 184–192.
[3] Gan, J., Zhang, X., Li, H., and Wu, H., 2017, "Full Closed-Loop Controls of Micro/Nano Positioning System With Nonlinear Hysteresis Using Micro-Vision System," Sens. Actuators A Phys., **257**, pp. 125–133.
[4] Tian, Y., Zhang, D., and Shirinzadeh, B., 2011, "Dynamic Modelling of a Flexure-Based Mechanism for Ultra-Precision Grinding Operation," Precis. Eng., **35**(4), pp. 554–565.
[5] Gozen, B. A., and Ozdoganlar, O. B., 2012, "Design and Evaluation of a Mechanical Nanomanufacturing System for Nanomilling," Precis. Eng., **36**(1), pp. 19–30.
[6] Lan, H., Ding, Y., Liu, H., and Lu, B., 2007, "Review of the Wafer Stage for Nanoimprint Lithography," Microelectron. Eng., **84**(4), pp. 684–688.
[7] Gu, G. Y., Zhu, L. M., Su, C. Y., Ding, H., and Fatikow, S., 2016, "Modeling and Control of Piezo-Actuated Nanopositioning Stages: A Survey," IEEE Trans. Autom. Sci. Eng., **13**(1), pp. 313–332.
[8] Clayton, G. M., Tien, S., Leang, K. K., Zou, Q., and Devasia, S., 2009, "A Review of Feedforward Control Approaches in Nanopositioning for High-Speed Spm," ASME J. Dyn. Syst., Meas., Control, **131**(6), pp. 636–650.
[9] Liu, L., Tan, K. K., Teo, C. S., Chen, S. L., and Tong, H. L., 2013, "Development of an Approach Toward Comprehensive Identification of Hysteretic Dynamics in Piezoelectric Actuators," IEEE Trans. Control Syst. Technol., **21**(5), pp. 1834–1845.
[10] Guo, Z., Tian, Y., Liu, X., Shirinzadeh, B., Wang, F., and Zhang, D., 2015, "An Inverse Prandtl–Ishlinskii Model Based Decoupling Control Methodology for a 3-DOF Flexure-Based Mechanism," Sens. Actuators A Phys., **230**, pp. 52–62.
[11] Ryba, L., Voda, A., and Besancon, G., 2015, "Experimental Comparison of Disturbance Observer and Inverse-Based Hysteresis Compensation in 3D Nanopositioning Piezoactuation," Sens. Actuators A Phys., **236**(37 Suppl. 2), pp. 190–205.
[12] Ming, M., Feng, Z., Ling, J., and Xiao, X.-H., 2018, "Hysteresis Modelling and Feedforward Compensation of Piezoelectric Nanopositioning Stage With a Modified Bouc-Wen Model," Micro Nano Lett., **13**, pp. 1170–1174.
[13] Xu, Q., and Li, Y., 2010, "Dahl Model-Based Hysteresis Compensation and Precise Positioning Control of an XY Parallel Micromanipulator With Piezoelectric Actuation," ASME J. Dyn. Syst., Meas., Control, **132**(4), pp. 558–564.
[14] Gu, G. Y., Li, C. X., Zhu, L. M., and Su, C. Y., 2016, "Modeling and Identification of Piezoelectric-Actuated Stages Cascading Hysteresis Nonlinearity With Linear Dynamics," IEEE/ASME Trans. Mechatronics, **21**(3), pp. 1792–1797.
[15] Liu, L., Tan, K. K., Chen, S., Teo, C. S., and Tong, H. L., 2013, "Discrete Composite Control of Piezoelectric Actuators for High-Speed and Precision Scanning," IEEE Trans. Ind. Inf., **9**(2), pp. 859–868.
[16] Feng, Z., Ling, J., Ming, M., and Xiao, X.-H., 2017, "High-Bandwidth and Flexible Tracking Control for Precision Motion With Application to a Piezo Nanopositioner," Rev. Sci. Instrum., **88**(8), p. 085107.
[17] Yi, J., Chang, S., and Shen, Y., 2009, "Disturbance-Observer-Based Hysteresis Compensation for Piezoelectric Actuators," IEEE/ASME Trans. Mechatronics, **14**(4), pp. 456–464.
[18] Devasia, S., Eleftheriou, E., and Moheimani, S. O. R., 2007, "A Survey of Control Issues in Nanopositioning," IEEE Trans. Control Syst. Technol., **15**(5), pp. 802–823.
[19] Ling, J., Feng, Z., Ming, M., and Xiao, X., 2018, "Damping Controller Design for Nanopositioners: A Hybrid Reference Model Matching and Virtual Reference Feedback Tuning Approach," Int. J. Precis. Eng. Manuf., **19**(1), pp. 13–22.
[20] Russell, D., Fleming, A. J., and Aphale, S. S., 2015, "Simultaneous Optimization of Damping and Tracking Controller Parameters Via Selective Pole Placement for Enhanced Positioning Bandwidth of Nanopositioners," ASME J. Dyn. Syst., Meas., Control, **137**(10), p. 101004.

[21] Fleming, A. J., Aphale, S. S., and Moheimani, S. O. R., 2010, "A New Method for Robust Damping and Tracking Control of Scanning Probe Microscope Positioning Stages," IEEE Trans. Nanotechnol., **9**(4), pp. 438–448.
[22] Li, C. X., Ding, Y., Gu, G. Y., and Zhu, L. M., 2017, "Damping Control of Piezo-Actuated Nanopositioning Stages With Recursive Delayed Position Feedback," IEEE/ASME Trans. Mechatronics, **22**(2), pp. 855–864.
[23] Aphale, S. S., Ferreira, A., and Moheimani, S. O. R., 2013, "A Robust Loop-Shaping Approach to Fast and Accurate Nanopositioning," Sens. Actuators A Phys., **204**(24), pp. 88–96.
[24] Teo, Y. R., Yong, Y., and Fleming, A. J., 2018, "A Comparison of Scanning Methods and the Vertical Control Implications for Scanning Probe Microscopy," Asian J. Control, **20**(4), pp. 1352–1366.
[25] Francis, B., and Wonham, W. M., 1976, "The Internal Model Principle of Control Theory," Automatica, **12**(5), pp. 457–465.
[26] Shan, Y., and Leang, K. K., 2012, "Dual-Stage Repetitive Control With Prandtl-Ishlinskii Hysteresis Inversion for Piezo-Based Nanopositioning," Mechatronics, **22**(3), pp. 271–281.
[27] Feng, Z., Ling, J., Ming, M., and Xiao, X., 2018, "A Model-Data Integrated Iterative Learning Controller for Flexible Tracking With Application to a Piezo Nanopositioner," Trans. Inst. Meas. Control, **40**(10), pp. 3201–3210.
[28] Wang, Y., Gao, F., and Doyle, F. J., 2009, "Survey on Iterative Learning Control, Repetitive Control, and Run-to-Run Control," J. Process Control, **19**(10), pp. 1589–1600.
[29] Zhou, K., Wang, D., Zhang, B., Wang, Y., Ferreira, J. A., and Haan, S. W. H. D., 2007, "Dual-Mode Structure Digital Repetitive Control," Automatica, **43**(3), pp. 546–554.
[30] Zhou, K., Wang, D., Zhang, B., and Wang, Y., 2009, "Plug-in Dual-Mode-Structure Repetitive Controller for CVCF PWM Inverters," IEEE Trans. Ind. Electron., **56**(3), pp. 784–791.
[31] Chen, X., and Tomizuka, M., 2014, "New Repetitive Control With Improved Steady-State Performance and Accelerated Transient," IEEE Trans. Control Syst. Technol., **22**(2), pp. 664–675.
[32] Sariyildiz, E., and Ohnishi, K., 2014, "A Guide to Design Disturbance Observer," ASME J. Dyn. Syst., Meas., Control, **136**(2), pp. 2483–2488.
[33] Sayem, A. H. M., Cao, Z., and Man, Z., 2017, "Model Free Eso-Based Repetitive Control for Rejecting Periodic and Aperiodic Disturbances," IEEE Trans. Ind. Electron., **64**(4), pp. 3433–3441.
[34] Wu, M., Yu, P., Chen, X., and She, J., 2017, "Design of Repetitive-Control System With Input Dead Zone Based on Generalized Extended-State Observer," ASME J. Dyn. Syst., Meas., Control, **139**(7), p. 071008.
[35] Helfrich, B. E., Lee, C., Bristow, D. A., Xiao, X., Dong, J., Alleyne, A. G., Salapaka, S. M., and Ferreira, P. M., 2010, "Combined H_∞ Feedback Control and Iterative Learning Control Design With Application to Nanopositioning Systems," IEEE Trans. Control Syst. Technol., **18**(2), pp. 336–351.
[36] Li, C. X., Gu, G. Y., Yang, M. J., and Zhu, L. M., 2017, "High-Speed Tracking of a Nanopositioning Stage Using Modified Repetitive Control," IEEE Trans. Autom. Sci. Eng., **14**(3), pp. 1467–1477.
[37] Lee, C., and Salapaka, S. M., 2009, "Robust Broadband Nanopositioning: Fundamental Trade-Offs, Analysis, and Design in a Two-Degree-of-Freedom Control Framework," Nanotechnology, **20**(3), p. 035501.
[38] Tomizuka, M., 1987, "Zero Phase Error Tracking Algorithm for Digital Control," ASME J. Dyn. Syst., Meas., Control, **109**(1), pp. 65–68.
[39] Butterworth, J. A., Pao, L. Y., and Abramovitch, D. Y., 2012, "Analysis and Comparison of Three Discrete-Time Feedforward Model-Inverse Control Techniques for Nonminimum-Phase Systems," Mechatronics, **22**(5), pp. 577–587.
[40] Sariyildiz, E., and Ohnishi, K., 2014, "Stability and Robustness of Disturbance-Observer-Based Motion Control Systems," IEEE Trans. Ind. Electron., **62**(1), pp. 414–422.
[41] Gu, G. Y., Zhu, L. M., and Su, C. Y., 2014, "High-Precision Control of Piezoelectric Nanopositioning Stages Using Hysteresis Compensator and Disturbance Observer," Smart Mater. Struct., **23**(10), p. 105007.
[42] Postlethwaite, I., 1996, *Multivariable Feedback Control: Analysis and Design*, Wiley, New York.